Applied Catalysis B: Environmental 184 (2016) 35–43

Contents lists available at ScienceDirect

Applied Catalysis B: Environmental

journal homepage: www.elsevier.com/locate/apcatb

MnO_2 nanowires decorated with Au ultrasmall nanoparticles for the green oxidation of silanes and hydrogen production under ultralow loadings

Anderson G.M. da Silva[a], Camila M. Kisukuri[a], Thenner S. Rodrigues[a], Eduardo G. Candido[a], Isabel C. de Freitas[a], Alisson H.M. da Silva[b], Jose M. Assaf[b], Daniela C. Oliveira[c], Leandro H. Andrade[a,*], Pedro H.C. Camargo[a,*]

[a] Departamento de Química Fundamental, Instituto de Química, Universidade de São Paulo, Av. Prof. Lineu Prestes, 748, 05508-000 São Paulo, SP, Brazil
[b] Departamento de Engenharia Química, Universidade Federal de São Carlos, 13565-905 São Carlos, SP, Brazil
[c] Laboratório Nacional de Luz Síncrotron, 13083-970, Campinas, SP, Brazil

ARTICLE INFO

Article history:
Received 2 October 2015
Received in revised form 8 November 2015
Accepted 17 November 2015
Available online 28 November 2015

Keywords:
Gold nanoparticles
Ultrasmall
MnO_2
Controlled-synthesis
Silane oxidation

ABSTRACT

Although green catalytic transformations are very attractive, they often remain limited by low conversion percentages and selectivity. Here, we demonstrate that high catalytic performances (TOF = 590,000 h^{-1}) could be achieved towards the green oxidation of silanes and H_2 production under ultralow Au loadings (0.001–0.0002 mol% in terms of Au) employing H_2O as the oxidant, 25 °C as the reaction temperature, and MnO_2 nanowires decorated with ultrasmall Au NPs (3 nm) as catalysts. In addition to these high activities towards a variety of substrates, the MnO_2–Au NPs displayed good stability/recyclability, in which no morphological changes or loss of activity were observed even after 10 reaction cycles. The improved catalytic activities observed for the MnO_2–Au NPs can be assigned to: (i) the metal–support interactions, in which the presence of Au NPs could facilitate oxidative processes and thus yield high performances towards the oxidation of hydrosilanes; (ii) the significant concentration of $Au^{\delta+}$ species and oxygen vacancies at the catalyst surface that represent highly catalytically active sites towards oxidation reactions, and (iii) the Au NPs ultrasmall sizes at the MnO_2 surface that enable the exposure of high energy Au surface/facets, high surface-to-volume ratios, and their uniform dispersion. The MnO_2–Au NPs could be synthesized by a facile approach based on the utilization of MnO_2 nanowires as physical templates for Au deposition without any prior surface modification/functionalization steps. The utilization of supported ultrasmall Au NPs having controlled sizes and dispersion may inspire the design of novel catalysts capable of enabling high catalytic performances towards green transformations at ultralow metal loadings.

1. Introduction

Gold nanoparticles (Au NPs) have attracted increased interest in the field of heterogeneous catalysis due to their high catalytic activity and selectivity, being employed in a variety of organic reactions that include oxidation, reduction, and C–C coupling [1–4]. Among these transformations, the oxidation of hydrosilanes has attracted particular attention. Silanols are a key element in the production of silicon-containing materials (i.e., polymers) [5–7]. Generally, hydrosilanes are classically converted into silanols using strong and toxic oxidizing agents such as permanganate, dichromate, and peracids that lead to significant amounts of siloxanes and toxic byproducts [7,8]. On the other hand, Au supported materials have been reported as promising catalysts for the oxidation of hydrosilanes using mild and non-toxic oxidants such as water and oxygen [5,6,8–10].

The green oxidation of organic compounds [2,11–13] has emerged as a new frontier in heterogeneous catalysis as this transformation represents an eco-friendly approach based on the use of dioxygen (O_2), water, or hydrogen peroxide as the oxidant, non-toxic solvents such as water, low catalyst loadings, and mild temperature and pressure conditions [14–17]. Despite these very attractive features, green oxidations remain challenging owing to the low conversion percentages, selectivities, and substrate versatility [12]. Therefore, the development of novel catalysts displaying

* Corresponding authors.
E-mail addresses: leandroh@iq.usp.br (L.H. Andrade), camargo.bme@gmail.com, camargo@iq.usp.br (P.H.C. Camargo).

http://dx.doi.org/10.1016/j.apcatb.2015.11.023
0926-3373/

high activities towards green transformations, such as oxidation, becomes highly desirable.

In this paper, we describe the catalytic activity of MnO_2 nanowires decorated with ultrasmall Au NPs (NPs having diameters of 3 nm or less) [18] towards the green oxidation of hydrosilanes, which produces silanols and hydrogen gas (H_2). Owing to their morphology comprised of ultrasmall Au NPs (3 nm), we found that the MnO_2–Au NPs displayed high catalytic performances under ultralow Au loadings (0.001–0.0002 mol%). Interestingly, the MnO_2–Au NPs were synthetized by a facile approach, which was based on the utilization of MnO_2 nanowires as physical templates for Au deposition without the need of any prior surface modification/functionalization steps. This method enabled the uniform deposition of monodisperse Au NPs over the entire surface of the support (MnO_2). MnO_2 was chosen as a model support material due to their low cost, stability, and low toxicity [19,20]. Moreover, various methodologies have been reported for the synthesis of MnO_2 displaying controlled shapes [21–24]. Although approaches to the synthesis of hybrids between MnO_2 and metal NPs have been reported, most of them generally do not lead a precise control over particle size, monodispersity, particle distribution, and composition, which is crucial to optimize activities [25–29].

2. Experimental

2.1. Materials and instrumentation

Analytical grade chemicals chloroauric acid trihydrate ($HAuCl_4{\cdot}3H_2O$, 99.9%, Sigma–Aldrich), manganese sulfate monohydrate ($MnSO_4{\cdot}H_2O$, 99%, Sigma–Aldrich), potassium permanganate ($KMnO_4$, 99%, Sigma–Aldrich), ethylene glycol (EG, 99.8%, Sigma–Aldrich), sodium borohydride ($NaBH_4$, 98%, Sigma–Aldrich), polyvinylpyrrolidone (PVP, Sigma–Aldrich, M.W. 55,000 g/mol), dimethyl(phenyl) silane ($C_8H_{12}Si$, 98%, Sigma–Aldrich), dimethyl(phenethyl) silane ($C_{10}H_{16}Si$, 98%, Sigma–Aldrich) cyclohexyldimethylsilane ($C_8H_{18}Si$, 98%, Sigma–Aldrich) were used without further purification. Dimethyl(1-phenylethyl) silane ($C_8H_{12}Si$) and dimethyl(1-(naphthalen-2-yl) ethyl) silane ($C_{14}H_{18}Si$) were synthetized according to previously reported protocols [30]. All solutions were prepared using deionized water (18.2 MΩ).

The scanning electron microscopy (SEM) images were obtained using a JEOL field emission gun microscope JSM 6330F operated at 5 kV. The samples were prepared by drop-casting an aqueous suspension containing the nanostructures over a silicon wafer, followed by drying under ambient conditions. The high-resolution transmission electron microscopy (HRTEM) images were obtained with a JEOL JEM2100 microscope operated at 200 kV. Samples for HRTEM were prepared by drop-casting an aqueous suspension of the nanostructures over a carbon-coated copper grid, followed by drying under ambient conditions. UV–vis spectra were obtained from aqueous suspensions containing the nanostructures with a Shimadzu UV-1700 spectrophotometer. The Au atomic percentage was measured by flame atomic absorption spectrometry (FAAS) with a Shimadzu spectrophotometer, model AA-6300, equipped with an air-acetylene flame.

2.2. Synthesis of MnO_2 nanowires

The MnO_2 nanowires were obtained by a hydrothermal approach [23]. In a typical procedure, 0.4 g of $MnSO_4{\cdot}H_2O$ and 1.0 g of $KMnO_4$ were dissolved in 30 mL of deionized water. This solution was transferred to an 100 mL Teflon-lined stainless steel autoclave. The autoclave was heated and stirred at 140 °C for 19 h and then allowed to cooled down to room temperature. The nanowires were washed three times with ethanol (15 mL) and three times with water (15 mL) by successive rounds of centrifugation and removal of the supernatant, and finally dried at 80 °C for 6 h in air.

2.3. Synthesis of MnO_2 nanowires decorated with Au NPs (MnO_2–Au NPs)

Typically, 40 mg of MnO_2 nanowires and 13 mg of PVP were added to 10 mL of EG. The obtained suspension was transferred to a 25 mL round-bottom flask and kept under vigorous stirring at 90 °C for 20 min. Then, 1 mL of an 120 mM $NaBH_{4(aq)}$ and 1 mL of a 24 mM $AuCl_4^-{}_{(aq)}$ solutions were sequentially added to the reaction flask. This mixture was kept under vigorous stirring for another 1 h to produce MnO_2–Au NPs, which were washed three times with ethanol (15 mL) and water (15 mL) by successive rounds of centrifugation at 6000 rpm for 5 min and removal of the supernatant. After washing, the MnO_2–Au NPs were suspended in 40 mL of water.

2.4. Oxidation of hydrosilanes catalyzed by MnO_2–Au NPs

In a typical experiment, a mixture of the hydrosilane (0.025 mmol), H_2O (0.5 mL), and 50 μL of the suspension containing MnO_2–Au NPs (0.001 mol% in terms of Au) were transferred to a 2 mL microtube (*Epperndorf*®). This system was kept under stirring at room temperature for 1 h, in a *Thermomixer*®. Then, the MnO_2–Au NPs was recovered from the reaction mixture by centrifugation and the supernatant was analyzed by GC–MS. GCM-QP2010SE Shimadzu instrument with low-resolution electron impact (EI, 70 eV) equipped with a RTx®-5MS capillary column. GC/MS conditions: injector 260 °C; detector: 110 °C pressure: 100 kPa. Column temperature: 80 °C, 1 °C/min up to 280 °C. The reaction products, when needed, were purified by a column chromatography (silica gel). The recovered catalyst was washed with water (3 × 1 mL) and re-used for the recycling studies.

3. Results and discussion

Our studies started with the synthesis of MnO_2 nanowires by a hydrothermal approach. The nanowires displayed well-defined shapes and uniform sizes, being 34 ± 5 nm in width and >1 μm in length (Fig. S1). The MnO_2 nanowires could be directly employed as physical templates for the nucleation and growth of Au NPs over their surface without the need of any surface modification/functionalization steps as depicted in Fig. 1A. Our approach employed $AuCl_4^-{}_{(aq)}$ as the Au precursor, PVP as the stabilizer, $BH_4^-{}_{(aq)}$ as the reducing agent, EG (ethylene glycol) as the solvent, and 90 °C as the reaction temperature. Fig. 1B–E shows HRTEM images of the MnO_2 nanowires decorated with Au NPs (MnO_2–Au NPs) obtained by this procedure. The uniform deposition (without agglomeration) of monodisperse, spherical, and ultrasmall (3 ± 1 nm) Au NPs over the entire surface of the MnO_2 nanowires could be clearly detected. Fig. 1D and E suggest that the Au NPs were directly deposited over the surface of the MnO_2 nanowires, and no morphology changes at the surface of the MnO_2 upon the formation of Au NPs could be observed. The MnO_2 were crystallized as β-MnO_2 and were single-crystalline, with its growing direction corresponding to {110} [23,31]. The characteristic lattice fringes from *fcc* Au can also be observed in Fig. 1E, and indicate that the Au NPs were single-crystalline. The Au content in the MnO_2–Au NPs suspension as determined by FAAS analysis corresponded to 0.17 mg/L. The XRD pattern for the MnO_2–Au NPs (Fig. S2) showed four peaks corresponding to the (1 1 0), (1 0 1), (2 1 1) and (2 0 0) reflections of the β-MnO_2 phase (JCPDS 24-0735). Only a small and broad peak assigned to the (1 1 1) reflection of *fcc* Au can be detected, in agreement with their ultrasmall sizes and low loading on the MnO_2 nanowires.

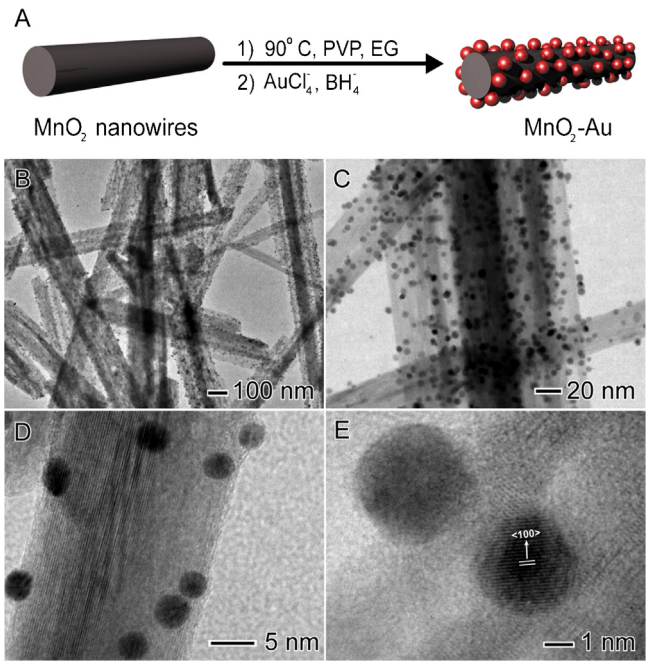

Fig. 1. (A) Strategy for the synthesis of MnO_2 nanowires decorated with ultrasmall Au NPs, which was based on the reduction of $AuCl_4^-{}_{(aq)}$ to Au by BH_4^- in presence of PVP, EG as the solvent, and 90 °C as the reaction temperature. (B–E) HRTEM images of MnO_2–Au NPs depicting the ultrasmall and monodisperse Au NPs size as well as their uniform distribution over the MnO_2 surface. The lattice fringe orientations in the phase-contrast HRTEM images (D and E) show that both the MnO_2 nanowires and Au NPs were single crystalline.

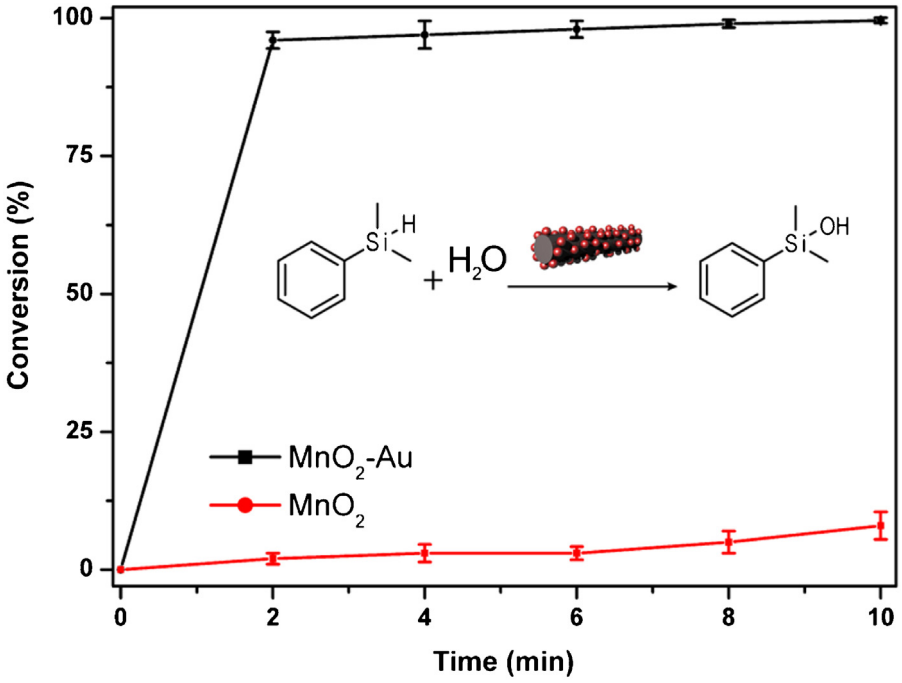

Fig. 2. Green oxidation of dimethyl(phenyl) silane catalyzed by MnO_2–Au NPs (black trace) and pure MnO_2 nanowires (red trace). Reaction profile was expressed as the conversion percentages (%) as a function of time. The reaction was carried out at 25 °C, employing water as the solvent, and the Au loading corresponded to 0.001 mol%. (For interpretation of the references to color in this figure legend, the reader is referred to the web version of this article).

Owing to the well-defined morphology comprised of micrometer long MnO_2 nanowires and ultrasmall Au NPs sizes, the MnO_2–Au NPs are very attractive for catalytic applications. We were particularly interested in investigating the catalytic activities of the MnO_2–Au NPs under ultralow Au loading conditions towards the green oxidation of hydrosilanes to silanol and gaseous hydrogen (H_2), using water as the solvent and under room temperature. Fig. 2 and Table 1 (entry 1) depict the conversion percentages (%) for the oxidation of dimethyl(phenyl) silane, employed as a model substrate, catalyzed by MnO_2–Au NPs. The catalyst loading in terms of Au corresponded to 0.001 mol%. While no significant conversion was detected for the MnO_2 nanowires after 10 min of reaction (control experiment), the MnO_2–Au NPs catalyst displayed high catalytic activities, achieving 97% of conversion after only 2 min,

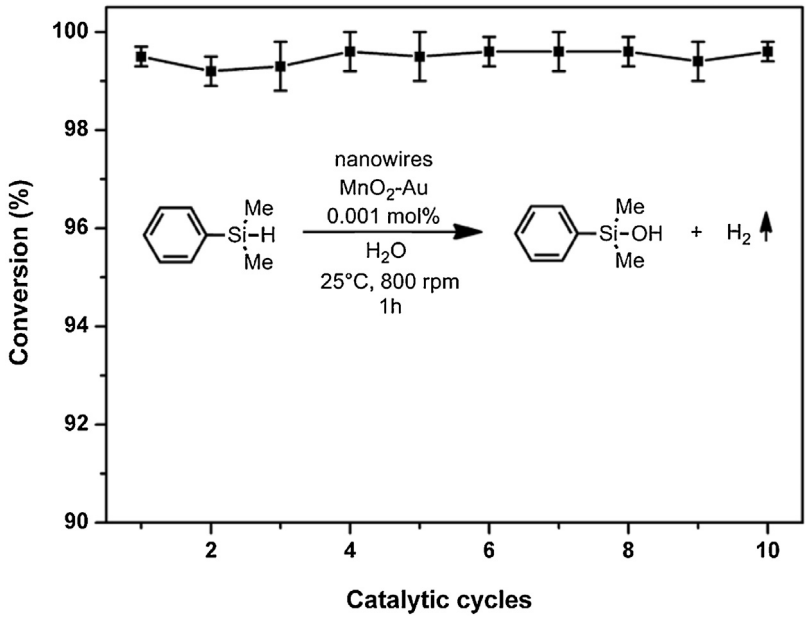

Fig. 3. Recycling/stability studies employing MnO_2–Au NPs as catalysts in the green oxidation of dimethylphenylsilane under the same conditions as described in Fig. 2. No significant loss of activity was observed even after 10 reaction cycles.

Table 1
Green oxidation of silanes catalyzed by MnO_2–Au NPs.[a]

Entry	R^1	Au loading (mol%)	Time (min)	Conversion[b] (%)	Selectivity to silanol[b] (%)
1	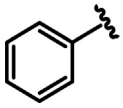	0.0002	60	90	100
2	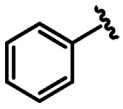	0.001	10	100	100
3	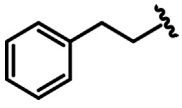	0.001	60	100	100
4	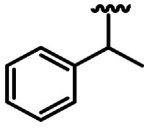	0.001	60	100	100
5	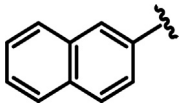	0.001	60	100	100
6	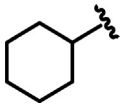	0.001	60	99	100

[a] Reactions conditions: silane (0.025 mmol), H_2O (0.5 mL), 25 °C, 800 rpm. All reactions were performed in duplicate. The percentage of catalyst was calculated based on the Au loading.
[b] The conversion and selectivity % were calculated using GC–MS analysis.

and 100% after 10 min. When the catalyst loading in terms of Au was further reduced to 0.0002 mol% (entry 2, Table 1), the MnO_2–Au NPs were still exceptionally active under our employed conditions, in which 90% conversion could be achieved after 60 min.

In order to demonstrate the versatility of the MnO_2–Au NPs as catalysts for the oxidation of hydrosilanes, we varied the nature of the groups attached to the Si atom, from arylic to benzylic groups (entry 3, Table 1). In this case, 100% conversion could be achieved after 60 min. This slightly difference in the silane structure possibly increases the steric hindrance at silicon atom, which could decrease the catalytic activity, since benzyldimethylsilanol was obtained in 100% after 10 min. The same behavior was observed for dimethyl(1-phenylethyl) silane (entry 4, Table 1). The dimethyl(naphthalen-2-yl) silane and cyclohexyldimethylsi-

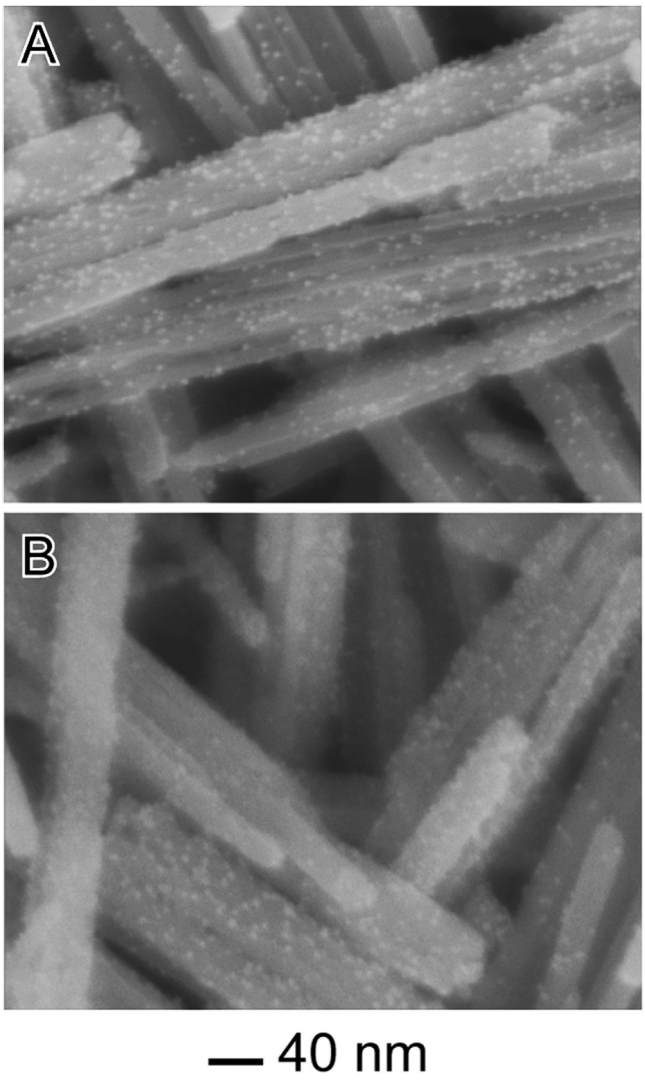

Fig. 4. SEM images of MnO_2–Au NPs catalysts before (A) and after (B) the recycling/stability studies described in Fig. 3, suggesting no significant morphological changes and indicating the robustness of the catalysts.

lane were also investigated as substrates (entries 5 and 6, Table 1, respectively). Both compounds were also successfully oxidized to silanol after 1 h (100% yield), suggesting that the MnO_2–Au NPs were efficient and versatile as catalysts in the oxidation of a variety of hydrosilanes under ultralow Au loading conditions. Ultralow can be defined as reactions catalyzed employing less than 0.1 mol% in terms of metal loadings [32,33].

One of the main advantages of heterogeneous as compared to homogeneous catalysis is the easy separation of the catalysts from the reaction mixture and its subsequent reusability. Here, the stability and recycling of the MnO_2–Au NPs catalysts towards the oxidation of dimethyl(phenyl) silane were investigated as depicted in Fig. 3. After each reaction cycle, the MnO_2–Au NPs catalysts were removed from the reaction mixture by centrifugation and washed before being reused in the next reaction cycle. In this case, the catalytic reactions were scaled-up by 20 folds. It can be observed that almost 100% conversion was achieved even after the 10th cycle, suggesting that the catalytic activities remained unaffected and the successive reaction cycles did not lead to any detrimental structural modifications on the MnO_2–Au NPs catalysts. The SEM images of the MnO_2–Au NPs before and after the catalytic tests (Fig. 4A and B, respectively) are in agreement with this observation, showing no change on the morphological features after the

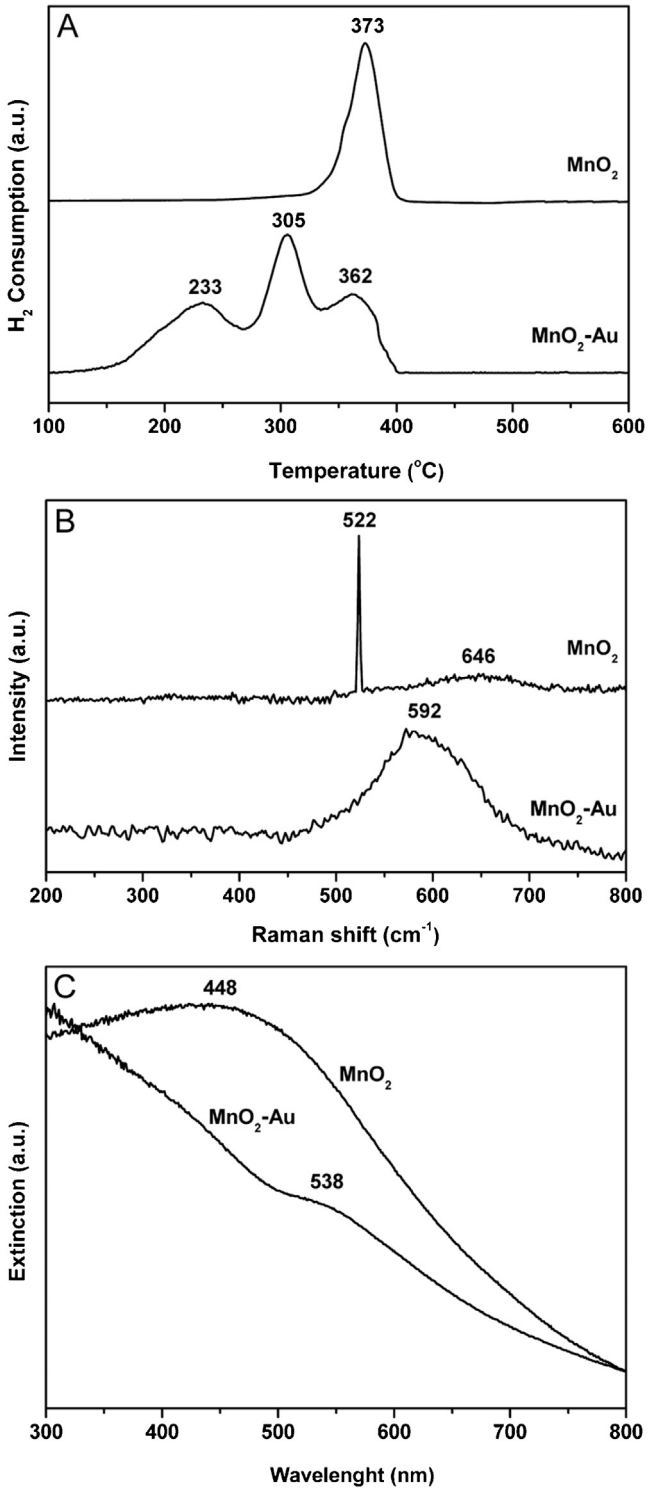

Fig. 5. Temperature programmed reduction profiles (A), Raman (B), and UV–vis (C) spectra for MnO_2 nanowires and MnO_2–Au NPs.

stability studies. We also evaluated the absence of Au leaching from the MnO_2–Au NPs under our experimental conditions by a series of control experiments. In this case, MnO_2–Au NPs were rapidly isolated during the course of the reaction (after 1 min of reaction) to avoid re-deposition of potentially leached metal ions onto the solid. Then, the supernatant was allowed to react even further. As expected for a heterogeneous mechanism, no further conversion of dimethyl(phenyl) silane was observed after removing the

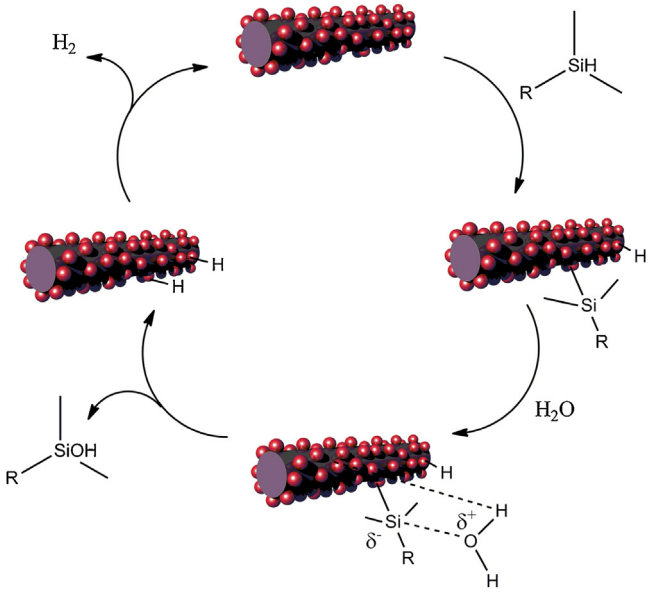

Scheme 1. Proposed mechanism for silane oxidation and hydrogen production reactions catalyzed by MnO_2–Au NPs.

MnO_2–Au NPs catalyst from the reaction mixture (Fig. S3). Moreover, the supernatant obtained from these leaching tests and also from the recycling experiments were quantified by FAAS analyses and Au was not detected.

No silane conversion was observed in the absence of H_2O, indicating that H_2O may act as the main oxidant in agreement with previous results [34]. In absence of O_2, a significant decrease in the reaction rate was observed (~50% in the dimethyl(phenyl) silane oxidation). This result suggests that O_2 molecules could react with the hydride species adsorbed at the catalyst surface, making them reactive for the next silane insertion according to the proposed mechanism depicted in Scheme 1 [34,35].

The deposition of noble metals over MnO_2 enabled improved eletrocatalytic and surface-enhanced Raman scattering performances due to metal–support interactions [36,37]. Moreover, Au NPs can interact with metal oxides to facilitate oxidative processes, in which the reducibility of the support material can play an important role over the observed performances [25]. Therefore, in order to gain further insights into the role played by the metal–support interactions over the high catalytic activities observed herein, the MnO_2 nanowires and MnO_2–Au NPs were investigated by temperature programmed reduction (TPR) and Raman and UV–vis spectroscopies (Fig. 5A–C, respectively). The TPR profile for the MnO_2 nanowires exhibited only a single and narrow reduction peak centered at 373 °C. Interestingly, the TPR profile was dramatically different for the MnO_2–Au NPs. In this case, reduction of MnO_2 support was facilitated and three main reduction steps corresponding to the reduction of MnO_2 to Mn_2O_3 (233 °C), Mn_2O_3 to Mn_3O_4 (305 °C), and then Mn_3O_4 to MnO (362 °C) could be observed [25]. This result clearly suggests that strong metal–support interactions take place in the MnO_2–Au NPs, in which the presence of ultrasmall Au NPs facilitated/promoted the MnO_2 reduction [25,38]. Raman and UV–vis spectroscopies (Fig. 5B and C, respectively) are in agreement with these observations. The Raman spectra for MnO_2 (Fig. 5B) displayed 522 and 646 nm signals assigned to the characteristic MnO_2 vibration modes. On the other hand, only a broad band centered at 592 nm was observed for the MnO_2–Au NPs, which can be explained by the distortion of the Mn–O–Mn chain in the octahedral manganese oxide lattice by the presence of Au, leading to loss of translational symmetry that activates otherwise Raman-forbidden oxygen vibrations [36]. Therefore, this broad band in the Raman spectra due to the presence Au reflect the phonon density of states rather than the Raman-allowed zone center phonons in MnO_2 [36]. The UV–vis spectra for MnO_2 nanowires displayed a broad band at 448 nm assigned to the *d*–*d* transitions (Fig. 5C) [39]. This signal was suppressed for MnO_2–Au NPs, while a broad and peak centered at 538 nm which is assigned to the dipole mode of the localized surface plasmon resonance excitation SPR in Au [40], in agreement with the Au NPs deposition over MnO_2 nanowires.

In order to gain further insights into the surface composition, oxidation state and the charge transfer tendencies between Au and MnO_2, both MnO_2 nanowires and MnO_2–Au NPs were investigated by XPS as depicted in Fig. 6A–C (XPS spectra) and Table 2 (XPS parameters and assignments). Mn 2p and Au 4f core levels presented well-separated spin-orbit components at $\Delta \sim 11.5$ and 3.7 eV, respectively. The binding energies (BE) of Au $4f_{7/2}$ and Mn $2p_{3/2}$ regions indicated slight shifts relative to bulk Au (84.0 ± 0.2 eV) and Mn (462.4 ± 0.2 eV) which can be explained due to the formation of nanosized particles that generally modify surface properties. In order to probe the surface structural and compositional changes that may occur during the Au deposition onto the MnO_2 surface, the Mn 2p, and O 1s XPS spectra were included for MnO_2 nanowires and MnO_2–Au NPs. The XPS spectrum for the MnO_2 nanowires (Fig. 6A) displays its main peak at the Mn $2p_{3/2}$ region centered at 642.9 eV, which can be to the presence of Mn^{4+} species in good agreement with XRD analysis [38,41]. Interestingly, a variation in the oxidation states of Mn species was observed after the Au NPs deposition at MnO_2 surface. In this case, the main peak at the Mn $2p_{3/2}$ region was shifted and broadened to 641.8 eV, which indicates the presence of Mn species in lower oxidation states, and thus the partial reduction of Mn^{4+} to $Mn^{\delta+}$ ($\delta < 4$) at the surface [42]. One plausible explanation for the observed reduction of Mn^{4+} species at the surface is the utilization of sodium borohydride (a reducing agent) during the Au NPs deposition step. However, this detected shift to lower binding energy region is also expected due to the charge transfer at the metal–support interface as a result of metal–support interactions [42,43].

The O 1s XPS spectra obtained from MnO_2 and MnO_2–Au NPs catalysts are shown in Fig. 6B. Three surface oxygen species could be observed in the O 1s XPS spectra. The binding energy between 529.9–529.5 eV was characteristic of the lattice oxygen (denoted as O_L), the binding energies between 532.0–531.4 eV were assigned to oxygen vacancies or the surface oxygen ions (denoted as O_s), and the binding energies around 533.9 eV were characteristic of adsorbed water (O_w) [41]. As expected, the analyses of O 1s XPS spectra are in agreement with the Mn $2p_{3/2}$ XPS results. The Au NPs deposition led to a decrease in the O_L/O_s ratio, demonstrating the enrichment of oxygen vacancies or the surface oxygen ions probably induced by the partial reduction of MnO_2 in presence of sodium borohydride during the Au NPs deposition step and/or charge transfer from Au to MnO_2 due to metal–support interactions [37,42,43]. Although manganese oxide is very stable, sodium borohydride is a strong reducing agent. Therefore, it is plausible that it can also partially reduce MnO_2 at the surface to lower oxidation states during the Au NPs deposition step, which is in agreement with XPS, HRTEM (demonstrating that the nanowire structure remained unaffected), and XRD (indicating that the main crystalline phase in the catalyst is β-MnO_2 phase) results.

In addition to partial MnO_2 reduction that led to an increase concentration of oxygen ions at their surface, the Au 4f XPS spectra (Fig. 6C) for the MnO_2–Au NPs displayed broad peaks in the Au 4f region, suggesting the presence of different oxidation states (Au^0 and $Au^{\delta+}$ species) [44]. In order to quantify these differences, the Au $4f_{7/2}$ region was de-convoluted into 2 peaks: one at 83.7 eV assigned to Au^0 species and other at 85.2 eV related to $Au^{\delta+}$ species.

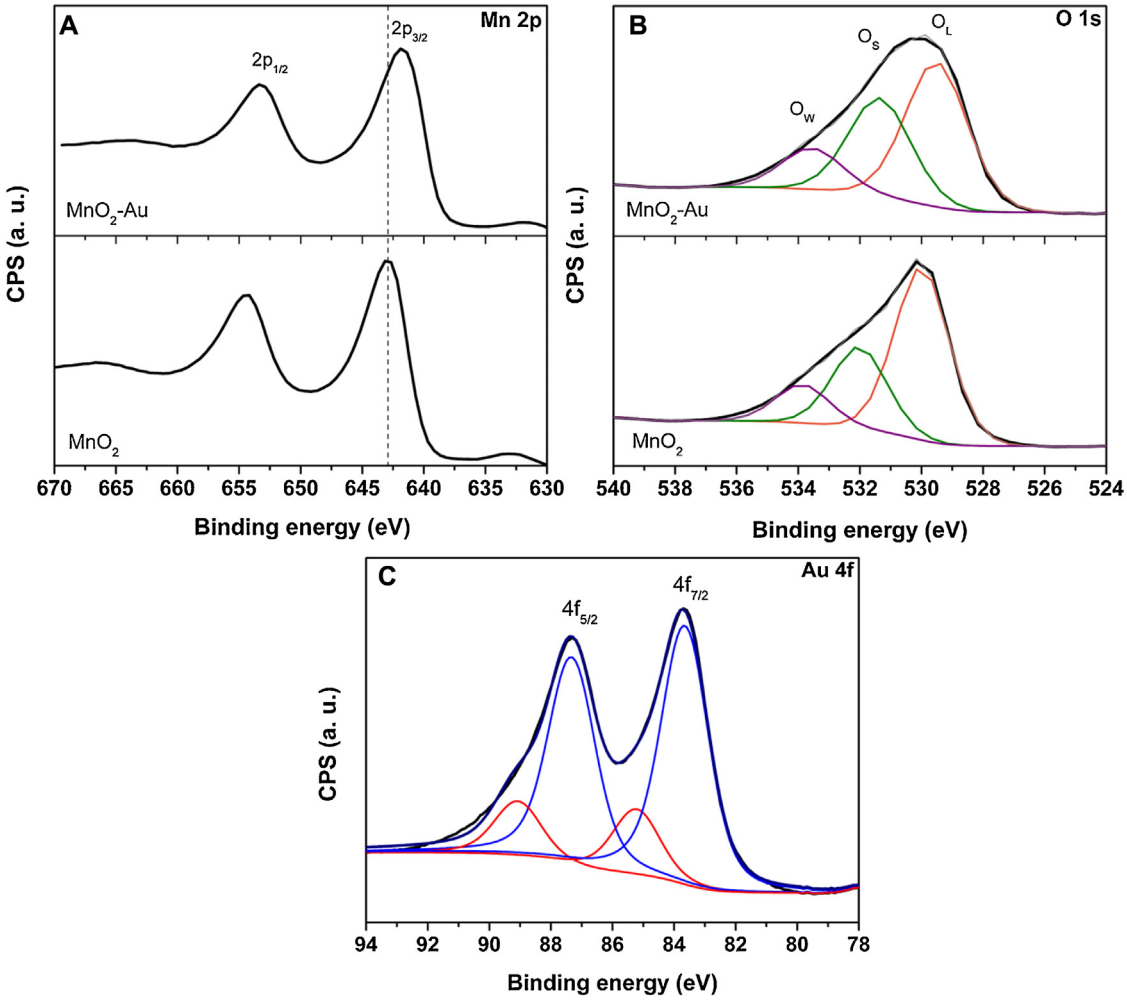

Fig. 6. XPS spectra of Mn 2p (A), O 1s (B) and Au 4f core levels for MnO_2 nanowires and MnO_2–Au NPs.

Table 2
Binding energies, surface composition, and Au:Mn ratio for MnO_2 nanowires and MnO_2–Au NPs measured by XPS analyses.

Catalyst	BE of Au $4f_{7/2}$ (eV)		BE of Mn $2p_{3/2}$ (eV)	BE of O 1s (eV)			Au:Mn
	Au^0	$Au^{\delta+}$		O_L	O_S	O_W	
MnO_2	no signal	no signal	642.9	529.9 (59)[a]	532.0 (28)[a]	533.9 (13)[a]	N/A
MnO_2–Au	83.7 (80)[a]	85.2 (20)[a]	641.8	529.5 (51)[a]	531.4 (35)[a]	533.6 (14)[a]	0.30

[a] Percent of Au or O species.

As depicted in Table 2, the Au NPs deposition at the MnO_2 surface led to the formation of a significant concentration of $Au^{\delta+}$ species. For instance, the $Au^{\delta+}/Au^0$ ratio was ~20% in the MnO_2–Au NPs. Experimental and theoretical studies on Au-based catalysts have demonstrated that the most catalytically active sites in oxidation reactions correspond to $Au^{\delta+}$ surface species [44,45]. Remarkably, our catalyst displayed a higher number of $Au^{\delta+}$ surface species relative to other reported Au-based catalysts displaying high activities towards oxidation reactions [4,38,46,47].

Therefore, we believe that the improved catalytic activities observed for the MnO_2–Au NPs can be assigned to: (i) the metal–support interactions, in which the presence of Au NPs could facilitate oxidative processes and thus yield high performances towards the oxidation of hydrosilanes; (ii) the significant concentration of $Au^{\delta+}$ species and oxygen vacancies at the catalyst surface that represent highly catalytically active sites towards oxidation reactions, and (iii) the Au NPs ultrasmall sizes at the MnO_2 surface that enable the exposure of high energy Au surface/facets (Fig. S4), high surface-to-volume ratios, and their uniform dispersion. The catalytic activity, reusability, and low Au loadings described herein for the MnO_2–Au catalysts agree with the principles of Green Chemistry applied to nanoscience, which encompasses the design of safer nanomaterials that can both meet performance specifications and may pose minimal health/environmental impacts [48]. Although Au NPs supported on different substrates can also catalyze this transformation, the MnO_2–Au NPs catalysts described in this paper displayed significantly improved catalytic performances relative to a conventional Au–SiO_2 material prepared by wet impregnation [49] and other systems containing Au NPs described in the literature as depicted in Table 3 [5,7–10,34]. For instance, MnO_2–Au NPs displayed significantly higher catalytic activities (TOF = 590,000 h^{-1}) relative to conventional Au–SiO_2 catalysts (TOF = 1534 h^{-1}) under lower metal loadings (0.001 mol Au% and 0.1 mol% for MnO_2–Au NPs and Au–SiO_2, respectively) [49]. Moreover, Au loading and the TOF value obtained for the MnO_2–Au NPs catalysts were much higher relative to Au NPs supported on carbon nanotubes,

Table 3
Oxidation of dimethyl(phenyl) silane in different solvents over MnO_2–Au NPs[a] and other catalysts reported in literature.

Catalysts	Au loading (mol%)	Solvent	Time (min)	Conversion (%)	TOF (h^{-1})	Refs.
MnO_2–Au	0.001	Water	10	>99	590000[b]	This work
Au–SiO_2	0.1	Water	10	23	1534	This work
Au–SiO_2	0.1	Water	60	>99	983	This work
AuHPA	0.83	Water	180	>99	40[b]	Ref. [5]
SBA–PIL–Au	0.4	Water	180	>99	83[b]	Ref. [7]
AuCNT	0.1	THF	45	98	72000	Ref. [8]
Au/SiO_2	0.4	THF	10	>99	14850[b]	Ref. [9]
AuNPore	1.0	Acetone	60	>99	10800[b]	Ref. [10]
Au-2	0.1	Water	40	>99	10167[b]	Ref. [34]

[a] Reactions conditions: silane (0.025 mmol), H_2O (0.5 mL), 25 °C, 800 rpm. All reactions were performed in duplicate.
[b] TOF based on the gold loading.

SiO_2, SBA-15, AlO(OH), and hydroxyapatite [5,7–10,34]. While the synthetic routes to produce these systems were relatively complicated and presented several steps, our approach to MnO_2–Au NPs was straightforward and enabled the synthesis of a relatively large amount of nanomaterial (40 mg per batch; reaction volume: 12 mL). In addition, the synthesis and catalytic TOF for the described MnO_2–Au NPs were reproducible and checked several times during our studies.

4. Conclusions

We have demonstrated that MnO_2 nanowires decorated with ultrasmall Au NPs (NPs having diameters of 3 nm or less) can be employed as heterogeneous catalysts towards the green oxidation of hydrosilanes and H_2 production. Surprisingly, we observed that high catalytic performances (TOF = 590,000 h^{-1}) could be achieved towards hydrosilane oxidation employing ultralow Au loadings (0.001–0.0002 mol% in terms of Au), water as solvent and oxidant, and at room temperature. Moreover, the MnO_2–Au NPs displayed good stability/recyclability, and no morphological changes or loss of activity were observed even after 10 reaction cycles. The MnO_2–Au NPs catalysts were comprised of MnO_2 nanowires 34 ± 5 nm in width and >1 μm in length, which could be directly employed as templates for the deposition of ultrasmall Au NPs over their surface employing $AuCl_4^-{}_{(aq)}$ as the Au precursor, $BH_4^-{}_{(aq)}$ as the reducing agent, PVP as the stabilizer, and ethylene glycol as the solvent. The Au NPs were uniformly deposited over the entire surface of the MnO_2 nanowires, displayed spherical shape, and were monodisperse. Moreover, their coverage/loading could be controlled by adjusting the amount of $AuCl_4^-{}_{(aq)}$ and $BH_4^-{}_{(aq)}$ added during the synthesis. Our results show that the utilization of supported ultrasmall Au NPs having controlled sizes and dispersion may inspire the design of novel catalysts capable of pushing the limits of Au heterogeneous catalysis, in which high catalytic performances towards green transformations can be achieved even at ultralow metal loadings.

Acknowledgments

This work was supported by the Fundação de Amparo à Pesquisa do Estado de São Paulo (FAPESP) (grant numbers 2013/19861 and 2014/22457-5) and the Conselho Nacional de Desenvolvimento Científico e Tecnológico (CNPq, grant numbers 471245/2012-7 and 140956/2014-0). P.H.C.C. and L.H.A. thank the CNPq for research fellowships. A.G.M.S. and C.M.K. thank the CNPq and T.S.R. thanks CAPES for the fellowships. A.H.M.S. thanks Agência Nacional do Petróleo for the fellowships. We thank the Brazilian Synchrotron Light Laboratory (LNLS) for the access to the XPS facility.

Appendix A. Supplementary data

Supplementary data associated with this article can be found, in the online version, at http://dx.doi.org/10.1016/j.apcatb.2015.11.023.

References

[1] Y. Zhang, X. Cui, F. Shi, Y. Deng, Nano-gold catalysis in fine chemical synthesis, Chem. Rev. 112 (2011) 2467–2505.
[2] B.K. Min, C.M. Friend, Heterogeneous gold-based catalysis for green chemistry: low-temperature CO oxidation and propene oxidation, Chem. Rev. 107 (2007) 2709–2724.
[3] G. Zhang, Y. Peng, L. Cui, L. Zhang, Gold-catalyzed homogeneous oxidative cross-coupling reactions, Angew. Chem. Int. Ed. 48 (2009) 3112–3115.
[4] A.G.M. da Silva, H.V. Fajardo, R. Balzer, L.F.D. Probst, A.S.P. Lovón, J.J. Lovón-Quintana, et al., Versatile and efficient catalysts for energy and environmental processes: mesoporous silica containing Au, Pd and Au–Pd, J. Power Sources 285 (2015) 460–468.
[5] T. Mitsudome, A. Noujima, T. Mizugaki, K. Jitsukawa, K. Kaneda, Supported gold nanoparticlecatalyst for the selective oxidation of silanes to silanols in water, Chem. Commun. (2009) 5302–5304.
[6] M. Jeon, J. Han, J. Park, Transformation of silanes into silanols using water and recyclable metal nanoparticle catalysts, ChemCatChem 4 (2012) 521–524.
[7] L. Ma, W. Leng, Y. Zhao, Y. Gao, H. Duan, Gold nanoparticles supported on the periodic mesoporous organosilica SBA-15 as an efficient and reusable catalyst for selective oxidation of silanes to silanols, RSC Adv. 4 (2014) 6807–6810.
[8] J. John, E. Gravel, A. Hagège, H. Li, T. Gacoin, E. Doris, Catalytic oxidation of silanes by carbon nanotube–gold nanohybrids, Angew. Chem. Int. Ed. 50 (2011) 7533–7536.
[9] W. Li, A. Wang, X. Yang, Y. Huang, T. Zhang, Au/SiO_2 as a highly active catalyst for the selective oxidation of silanes to silanols, Chem. Commun. 48 (2012) 9183–9185.
[10] N. Asao, Y. Ishikawa, N. Hatakeyama, Menggenbateer, Y. Yamamoto, M. Chen, et al., Nanostructured materials as catalysts: nanoporous-gold-catalyzed oxidation of organosilanes with water, Angew. Chem. Int. Ed. 49 (2010) 10093–10095.
[11] C.L. Hill, Homogeneous catalysis: controlled green oxidation, Nature 401 (1999) 436–437.
[12] R.A. Sheldon, Fundamentals of green chemistry: efficiency in reaction design, Chem. Soc. Rev. 41 (2012) 1437–1451.
[13] C. Parmeggiani, F. Cardona, Transition metal based catalysts in the aerobic oxidation of alcohols, Green Chem. 14 (2012) 547–564.
[14] C. Wen, A. Yin, W.-L. Dai, Recent advances in silver-based heterogeneous catalysts for green chemistry processes, Appl. Catal. B Environ. 160–161 (2014) 730–741.
[15] V. Polshettiwar, R.S. Varma, Green chemistry by nano-catalysis, Green Chem. 12 (2010) 743–754.
[16] R.A. Sheldon, I.W.C.E. Arends, G.-J. ten Brink, A. Dijksman, Green, catalytic oxidations of alcohols, Acc. Chem. Res. 35 (2002) 774–781.
[17] T.S. Rodrigues, A.G.M. da Silva, M.C. Gonçalves, H.V. Fajardo, R. Balzer, L.F.D. Probst, et al., AgPt hollow nanodendrites: synthesis and uniform dispersion over SiO_2 support for catalytic applications, ChemNanoMat 1 (2015) 46–51.
[18] B.H. Kim, M.J. Hackett, J. Park, T. Hyeon, Synthesis, characterization, and application of ultrasmall nanoparticles, Chem. Mater. 26 (2014) 59–71.
[19] P. Yang, Y. Ding, Z. Lin, Z. Chen, Y. Li, P. Qiang, et al., Low-cost high-performance solid-state asymmetric supercapacitors based on MnO_2 nanowires and Fe_2O_3 nanotubes, Nano Lett. 14 (2014) 731–736.
[20] X. Lu, T. Zhai, X. Zhang, Y. Shen, L. Yuan, B. Hu, et al., WO_3–x@Au@MnO_2 core–shell nanowires on carbon fabric for high-performance flexible supercapacitors, Adv. Mater. 24 (2012) 938–944.
[21] W. Xiao, D. Wang, X.W. Lou, Shape-controlled synthesis of MnO_2 nanostructures with enhanced electrocatalytic activity for oxygen reduction, J. Phys. Chem. C 114 (2010) 1694–1700.

[22] T.T. Truong, Y. Liu, Y. Ren, L. Trahey, Y. Sun, Morphological and crystalline evolution of nanostructured mno2 and its application in lithium-air batteries, ACS Nano 6 (2012) 8067–8077.
[23] X. Wang, Y. Li, Selected-control hydrothermal synthesis of α- and β-MnO_2 single crystal nanowires, J. Am. Chem. Soc. 124 (2002) 2880–2881.
[24] W.-M. Chen, L. Qie, Q.-G. Shao, L.-X. Yuan, W.-X. Zhang, Y.-H. Huang, Controllable synthesis of hollow bipyramid β-MnO_2 and its high electrochemical performance for lithium storage, ACS Appl. Mater. Interfaces 4 (2012) 3047–3053.
[25] M. Alhumaimess, Z. Lin, Q. He, L. Lu, N. Dimitratos, N.F. Dummer, et al., Oxidation of benzyl alcohol and carbon monoxide using gold nanoparticles supported on MnO_2 nanowire microspheres, Chem. Eur. J. 20 (2014) 1701–1710.
[26] A.K. Thapa, T.H. Shin, S. Ida, G.U. Sumanasekera, M.K. Sunkara, T. Ishihara, Gold–palladium nanoparticles supported by mesoporous β-MnO_2 air electrode for rechargeable Li-air battery, J. Power Sources 220 (2012) 211–216.
[27] K.-N. Jung, A. Riaz, S.-B. Lee, T.-H. Lim, S.-J. Park, R.-H. Song, et al., Urchin-like α-MnO_2 decorated with Au and Pd as a bi-functional catalyst for rechargeable lithium–oxygen batteries, J. Power Sources 244 (2013) 328–335.
[28] S.-Y. Liu, G. Wang, J. Xie, F. Tu, H. Yang, S. Zhang, et al., Au-nanocrystals-decorated [small delta]-MnO_2 as efficient catalytic cathode for high-performance Li-O_2 batteries, Nanoscale (2015), http://dx.doi.org/10.1039/C5NR01344E.
[29] T. Qiu, B. Luo, M. Giersig, E.M. Akinoglu, L. Hao, X. Wang, et al., Au@MnO_2 core–shell nanomesh electrodes for transparent flexible supercapacitors, Small 10 (2014) 4136–4141.
[30] A.R. Bassindale, J.C.-Y. Lau, P.G. Taylor, Nucleophile-assisted racemisation of halosilanes; an alternative pathway involving halide exchange, J. Organomet. Chem. 341 (1988) 213–224.
[31] A. Débart, A.J. Paterson, J. Bao, P.G. Bruce, α-MnO_2 nanowires: a catalyst for the O_2 electrode in rechargeable lithium batteries, Angew. Chem. 120 (2008) 4597–4600.
[32] Y. Jin, J. Xi, Z. Zhang, J. Xiao, F. Xiao, L. Qian, et al., An ultra-low Pd loading nanocatalyst with efficient catalytic activity, Nanoscale 7 (2015) 5510–5515.
[33] J.-C. Hierso, M. Beaupérin, P. Meunier, Ultra-low catalyst loading as a concept in economical and sustainable modern chemistry: the contribution of ferrocenylpolyphosphane ligands, Eur. J. Inorg. Chem. 2007 (2007) 3767–3780.
[34] T. Liu, F. Yang, Y. Li, L. Ren, L. Zhang, K. Xu, et al., Plasma synthesis of carbon nanotube-gold nanohybrids: efficient catalysts for green oxidation of silanes in water, J. Mater. Chem. A 2 (2014) 245–250.
[35] C. Shang, Z.-P. Liu, Origin and activity of gold nanoparticles as aerobic oxidation catalysts in aqueous solution, J. Am. Chem. Soc. 133 (2011) 9938–9947.
[36] S. Jana, S. Pande, A.K. Sinha, S. Sarkar, M. Pradhan, M. Basu, et al., A green chemistry approach for the synthesis of flower-like Ag-doped MnO_2 nanostructures probed by surface-enhanced raman spectroscopy, J. Phys. Chem. C. 113 (2009) 1386–1392.
[37] Y. Gorlin, C.-J. Chung, J.D. Benck, D. Nordlund, L. Seitz, T.-C. Weng, et al., Understanding interactions between manganese oxide and gold that lead to enhanced activity for electrocatalytic water oxidation, J. Am. Chem. Soc. 136 (2014) 4920–4926.
[38] L.-C. Wang, Y.-M. Liu, M. Chen, Y. Cao, H.- Yong, K.-N. Fan, MnO_2 nanorod supported gold nanoparticles with enhanced activity for solvent-free aerobic alcohol oxidation, J. Phys. Chem. C 112 (2008) 6981–6987.
[39] W. Li, X. Cui, R. Zeng, G. Du, Z. Sun, R. Zheng, et al., Performance modulation of α-MnO_2 nanowires by crystal facet engineering, Sci. Rep. 5 (2015), http://dx.doi.org/10.1038/srep08987.
[40] A.G.M. da Silva, T.S. Rodrigues, A. Macedo, R.T.P. da Silva, P.H.C. Camargo, An undergraduate level experiment on the synthesis of Au nanoparticles and their size-dependent optical and catalytic properties, Quim. Nova 37 (2014) 1716–1720.
[41] S. Liang, F. Teng, G. Bulgan, R. Zong, Y. Zhu, Effect of Phase structure of MnO_2 nanorod catalyst on the activity for CO oxidation, J. Phys. Chem. C 112 (2008) 5307–5315.
[42] L.-H. Chang, N. Sasirekha, Y.-W. Chen, W.-J. Wang, Preferential oxidation of CO in H_2 stream over Au/MnO_2-CeO_2 ctalysts, Ind. Eng. Chem. Res. 45 (2006) 4927–4935.
[43] H. Zhang, C. Lin, F. Du, Y. Zhao, P. Gao, H. Chen, et al., Enhanced interactions between gold and MnO_2 nanowires for water oxidation: a comparison of different chemical and physical preparation methods, ACS Sustain. Chem. Eng. 3 (2015) 2049–2057.
[44] M.P. Casaletto, A. Longo, A. Martorana, A. Prestianni, A.M. Venezia, XPS study of supported gold catalysts: the role of Au^0 and $Au^{+\delta}$ species as active sites, Surf. Interface Anal. 38 (2006) 215–218.
[45] L. Chen, J.M. Chabu, Y. Liu, Bimetallic AgM (M = Pt, Pd, Au) nanostructures: synthesis and applications for surface-enhanced Raman scattering, RSC Adv. 3 (2013) 4391–4399.
[46] T.J.A. Slater, A. Macedo, S.L.M. Schroeder, M.G. Burke, P. O'Brien, P.H.C. Camargo, et al., Correlating catalytic activity of Ag–Au nanoparticles with 3D compositional variations, Nano Lett. 14 (2014) 1921–1926.
[47] P. Sudarsanam, B. Mallesham, P.S. Reddy, D. Großmann, W. Grünert, B.M. Reddy, Nano-Au/CeO_2 catalysts for CO oxidation: influence of dopants (Fe, La and Zr) on the physicochemical properties and catalytic activity, Appl. Catal. B Environ. 144 (2014) 900–908.
[48] L.M. Gilbertson, J.B. Zimmerman, D.L. Plata, J.E. Hutchison, P.T. Anastas, Designing nanomaterials to maximize performance and minimize undesirable implications guided by the Principles of Green Chemistry, Chem. Soc. Rev. (2015), http://dx.doi.org/10.1039/c4cs00445k.
[49] A.G.M. da Silva, T.S. Rodrigues, T.J.A. Slater, E.A. Lewis, R.S. Alves, H.V. Fajardo, et al., Controlling size, morphology, and surface composition of AgAu nanodendrites in 15 s for improved environmental catalysis under low metal loadings, ACS Appl. Mater. Interfaces (2015), http://dx.doi.org/10.1021/acsami.5b08725.